PREDICTION OF MICROSCALE RESIN FLOW AND VOID FORMATION IN RESIN TRANSFER MOLDING USING A PARTICLE METHOD

Shigeki Yashiro[1] and Daichi Nakashima[2]

[1] Department of Aeronautics and Astronautics, Kyushu University
744 Motooka, Nishi-ku, Fukuoka 819-0395, Japan
Email: yashiro@aero.kyushu-u.ac.jp, Web Page: http://www.aero.kyushu-u.ac.jp/english/
[2] Graduate School of Integrated Science and Technology, Shizuoka University
3-5-1 Johoku, Naka-ku, Hamamatsu 432-8561, Japan
Web Page: http://www.eng.shizuoka.ac.jp/en/

Keywords: Resin transfer molding (RTM), Porosity, Surface tension, Wettability, Moving particle semi-implicit (MPS) method

Abstract
Prediction of void formation in the resin transfer molding (RTM) process will provide useful information such as the inhomogeneous microstructure and the mechanical properties of molded composite materials. This study aims at developing a numerical procedure to predict the resin flow with considering the microstructure of fiber preforms. Flow of liquids in imitated fiber bundles was first observed by using a transparent mold. The structure of the imitated fiber bundle was modeled by the moving particle semi-implicit (MPS) method, and liquid flow to the bundle was analyzed taking into account the surface tension and wettability as a potential force. Impregnation behavior depended on liquid properties, and the predicted process of void formation agreed well with the observation. This result indicated that the void content varied by the molding conditions such as the injection speed and liquid properties. Those molding conditions can be integrated into the capillary number (i.e., the ratio of the viscous force to the surface tension), and influence of this parameter on the void content was investigated analytically. The microscale flow analysis provided an appropriate molding condition to reduce voids with considering the fiber mat material and the resin.

1. Introduction

Fiber-reinforced plastics (FRPs) have frequently been applied to automobile structures in addition to aerospace structures to improve fuel consumption efficiency because of their light weight and good mechanical properties. Resin transfer molding (RTM) is promising owing to its high productivity compared to autoclave molding. FRPs obtained by RTM generally have high strength and stiffness. However, in some cases, voids are formed during the impregnation process, and these defects deteriorate the mechanical properties.

Micro- and macro-voids are observed depending on the molding condition. Micro-voids are tiny air residuals inside a fiber bundle, and macro-voids are large air pockets across fiber bundles. Rohatgi et al. [1] observed void formation process in a glass preform and measured void content. They found that the void content depended on the molding condition that was integrated into the modified capillary number.

This study then aims at predicting void formation during the resin filling process by a flow simulation considering the microstructure of the fiber preform. Impregnation is the flow along microscale paths,

and therefore, the surface tension of the resin and wettability to fibers will have great influence on the void formation. This study employs the moving particle semi-implicit (MPS) method to explicitly model the microstructure of fiber bundles and to analyze the microscale flow.

Liquid flow into simulated fiber bundles was first observed by using a transparent mold. A flow analysis corresponding to the experiment was then performed using the MPS method. The microstructure of the preform, the liquid and air are represented by an assembly of particles, and the liquid flow was predicted with considering a potential force for the surface tension and wettability, which was confirmed by a droplet collapse simulation.

2. Observation of void formation

Liquid flow to fiber bundles was observed by using a transparent mold. Figure 1 depicts schematic of the mold. The mold cavity was 22 mm wide and 1 mm thick. Quartz rods with a diameter of 1.0 mm were embedded in the mold to simulate fiber bundles. The minimum spacing between adjacent rods was 0.4 mm, and densely-arrayed rods were assumed as a fiber bundle.

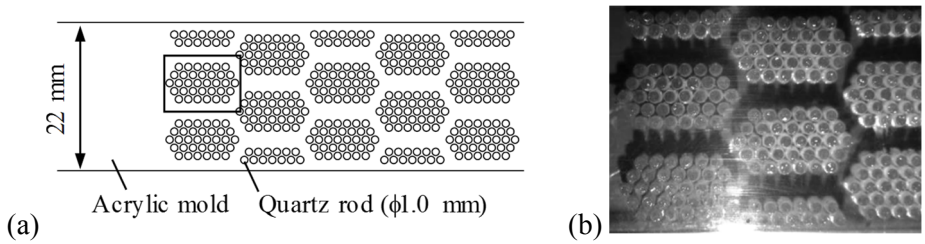

Figure 1. Transparent mold with embedded quartz rods: (a) schematic, and (b) magnified view.

Water and olive oil were injected to the mold, and the impregnation process was observed by a high-speed microscope (VW-9000, Keyence). The density and kinetic viscosity of the water were 1000 kg/m^3 and 1.0×10^{-6} m^2/s; these properties of the olive oils were 914 kg/m^3 and 8.37×10-5 m^2/s, which were measured by the Archimedes method and by the capillary viscometer method. Liquids were injected at a constant flow rate by using a micro-syringe pump (KDS-100, KD Scientific). The flow velocity in the empty space (i.e., before starting impregnation) was 6.3 mm/s. The bundle designated in Fig. 1 was observed in detail. The void fraction was determined as the area of voids divided by the observation area.

Figure 2 depicts the observed impregnation process in the case of water. The dotted line in these snapshots indicated the flow front. Water immersed only the outermost layer of the bundle, and then flowed mainly between bundles without infiltrating the bundles (Figs. 2a-2c). Under this experiment condition, the flow velocity between the bundles was higher than that in the bundle, and the bundle was

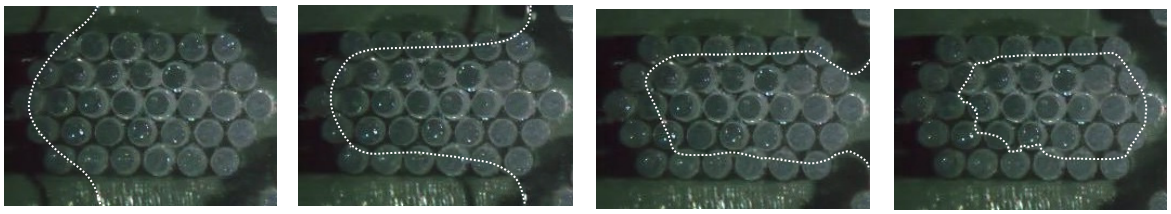

Figure 2. Snapshots of the water flow to a bundle. The dotted line indicates the flow front.

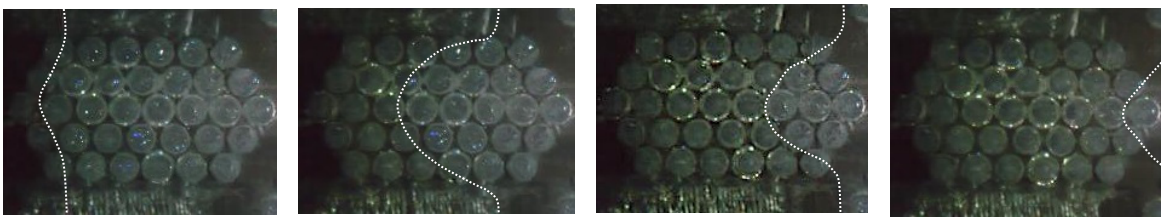

(a) 0.07 s (b) 0.60 s (c) 1.20 s (d) 1.53 s

Figure 3. Snapshots of the olive-oil flow to a bundle. The dotted line indicates the flow front.

surrounded by water before complete impregnation (Fig. 2d). A large amount of air remained inside the bundle, and the void fraction of the observed area was 10.8 %. Contrary to the water, the olive oil flowed into the bundle, and the flow front velocity in the bundle was only slightly lower than that between the bundles (Fig. 3). As a result, the bundle was completely filled before the bundle was surrounded by the olive oil, and no void was formed. This difference suggested that the surface tension and wettability greatly affected the flow to a fiber bundle as well as formation of voids.

3. Analysis

3.1. Moving particle semi-implicit (MPS) method

The MPS method [2] is a particle method, and continua such as fluids and solids are expressed as an assembly of particles. The governing equations of incompressible fluid are discretized by the differential operator models. When a particle i has a scalar variable ϕ_i, the gradient model is defined as

$$\left\langle \nabla \phi \right\rangle_i = \frac{d}{n^0} \sum_{j \neq i}^{N} \left[\frac{\phi_j - \phi_i}{\left| \mathbf{r}_j - \mathbf{r}_i \right|^2} \left(\mathbf{r}_j - \mathbf{r}_i \right) w\left(\left| \mathbf{r}_j - \mathbf{r}_i \right| \right) \right], \tag{1}$$

where d is the dimensional number, n^0 is the constant particle number density under the incompressible condition, $\mathbf{r}_i$ is the position vector of a particle i, N is the number of particles within the effective radius r_e of interaction, and w ($=r_e/r - 1$) is the weight function. The divergence model for the vector $\mathbf{u}$ is defined as

$$\left\langle \nabla \cdot \mathbf{u} \right\rangle_i = \frac{d}{n^0} \sum_{j \neq i}^{N} \left[\frac{\left(\mathbf{u}_j - \mathbf{u}_i \right) \cdot \left(\mathbf{r}_j - \mathbf{r}_i \right)}{\left| \mathbf{r}_j - \mathbf{r}_i \right|^2} w\left(\left| \mathbf{r}_j - \mathbf{r}_i \right| \right) \right]. \tag{2}$$

A part of a quantity ϕ of a particle i is distributed among neighboring particles j according to the distribution of the weight function by the Laplacian operation, and this model is represented as follows.

$$\left\langle \nabla^2 \phi \right\rangle_i = \frac{2d}{\lambda n^0} \sum_{j \neq i}^{N} \left[\left(\phi_j - \phi_i \right) w\left(\left| \mathbf{r}_j - \mathbf{r}_i \right| \right) \right] \tag{3}$$

$$\lambda = \int_{r_0}^{r_e} r^2 \left(\frac{r_e}{r} - 1 \right) 2\pi r \, \mathrm{d}r \Big/ \int_{r_0}^{r_e} \left(\frac{r_e}{r} - 1 \right) 2\pi r \, \mathrm{d}r \tag{4}$$

Here, λ is a constant to make the increase in statistical dispersion conform to the analytical solution.

The governing equations of incompressible flow are the mass conservation (equation of continuity) and the Navier-Stokes equation.

$$\frac{D\rho}{Dt} = 0 \tag{5}$$

$$\frac{D\mathbf{u}}{Dt} = -\frac{1}{\rho}\nabla P + \nu\nabla^2\mathbf{u} + \mathbf{g} \tag{6}$$

The viscous (2nd) term and the external force (3rd) term of the right-hand-side of the Navier-Stokes equation are solved explicitly, and the Poisson's equation of pressure derived from the pressure (1st) term and the mass conservation equation is solved implicitly. However, resulting pressure distribution frequently includes numerical oscillation. This study then employed an improved solving scheme [3] to obtain smooth pressure distribution.

3.2. Potential force model for the surface tension and wettability

An inter-particle potential Π is used to represent the surface tension:

$$\Pi(r) = C\,\pi(r), \tag{7}$$

where C and $\pi(r)$ is the coefficient and the potential function as a function of the distance between two particles, r. This study employed a potential function proposed by Kondo et al. [4] and the Morse potential, and verified their validity.

$$\pi(r) = \frac{1}{3}\left(r - \frac{3}{2}l_0 + \frac{1}{2}r_e\right)(r - r_e)^2 \tag{8}$$

$$\pi(r) = e^{-2(r/l_0-1)} - 2e^{-(r/l_0-1)} \tag{9}$$

Here, l_0 is the equilibrium particle distance (i.e., the initial particle distance of the particle model), and r_e is the effective radius of the potential.

Wettability can be represented by using two specific potential coefficients for interaction between two fluid particles and for interaction between a fluid particle and a solid one. This study assumes the following relation between the two coefficients:

$$C_2 = a\,C_1, \tag{10}$$

where C_1 and C_2 are the coefficients for fluid-fluid interaction and for fluid-solid interaction, and a is an arbitrary positive constant.

The inter-particle potential force $\mathbf{F}_s$ is given by the gradient of the potential.

$$\mathbf{F}_s = -\sum_{j\neq i}\frac{\partial\Pi(r)}{\partial r}\frac{\mathbf{r}_j - \mathbf{r}_i}{|\mathbf{r}_j - \mathbf{r}_i|} \tag{11}$$

The potential force was handled as an external force, and this term was added to the right-hand-side of Eq. (6), which was solved explicitly.

4. Analytical results and discussion

4.1. Verification of the potential force model

Droplet collapse was investigate experimentally and analytically to verify the inter-particle potential model for the surface tension and wettability. The angle of contact between liquids and a quartz plate was measured by an automatic contact angle meter (DMe-201, Kyowa Interface Science) based on a half-angle (θ/2) method. The contact angles of water and olive oil were 39.9° and 27.4°, respectively.

Droplet collapse was then analyzed using the inter-particle potential model, Eqs. (8) and (9). Figure 4a depicts the two-dimensional analytical model, and the size of a particle was 0.125 mm. Properties of liquids listed in Section 2 were used. The analysis time was 0.5 s. The contact angle of the analysis was determined by the $\theta/2$ method. The contact angle θ was calculated by

$$\theta = 2 \tan^{-1}(2H/W), \tag{12}$$

where H is the height of the collapsed droplet, and W is the width of the liquid at the interface between the plate and the liquid. The contact angle after 0.2 s, at which the motion of the droplet was almost converged, was averaged.

Figures 4b-4g depicts the finial state of the droplet at 0.5 s. The parameters C_1 and a in Eq. (10) were adjusted to fit the predicted contact angles to the experiment, and the obtained parameters and the predicted contact angle are listed in Table 1. Although the obtained contact angles agreed with the measurement in all cases, the potential model of Eq. (8) caused an unrealistic state such as aggregation of particles on the surface (Figs. 4b, 4c, 4e and 4f), detached particles (Fig. 4c) and concave shape at the ends of the droplet (Fig. 4e). The potential model of Eq. (9) improved the behavior of the droplet.

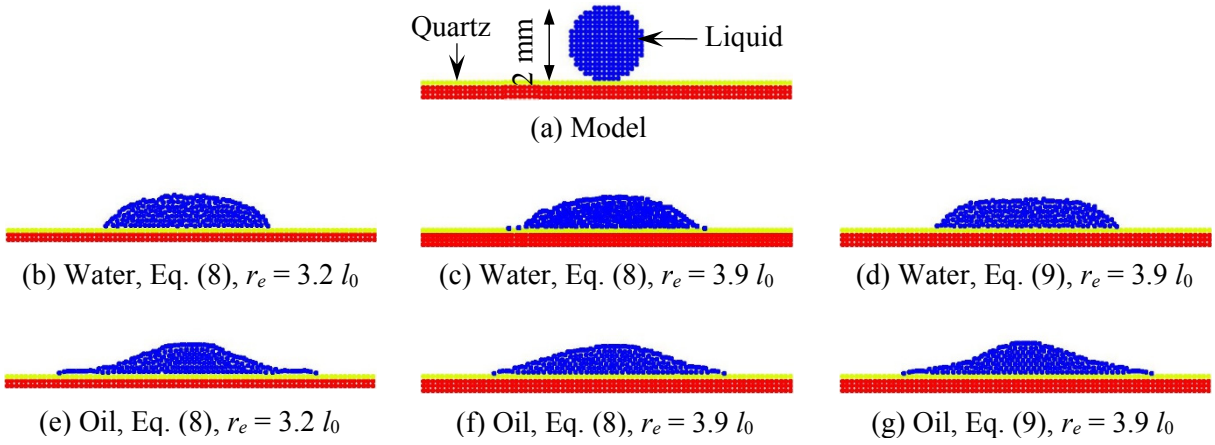

Figure 4. Converged state of the droplet collapse.

Table 1. Predicted contact angles in the droplet collapse analysis.

Liquid	Eq. (8), $r_e = 3.2l_0$			Eq. (8), $r_e = 3.9l_0$			Eq. (9), $r_e = 3.9l_0$			Measured
type	C_1	a	θ	C_1	a	θ	C_1	a	θ	θ
Water	20	0.72	39.9°	20	0.8	39.4°	20	0.73	38.3°	39.9°
Oil	200	1.245	28.4°	200	1.135	30.6°	200	1.215	30.7°	27.4°

4.2. Liquid flow in the fiber bundle

Two-dimensional analysis of the liquid flow to the fiber bundle corresponding to the experiment in Section 2 was performed to predict the void formation process. Figure 5 depicts the analytical model. The size of a particle was 0.125 mm, and a rod was represented by 52 particles. Total number of particles at the initial condition was 8364. Liquid particles were injected at a flow velocity of 6.3 mm/s from the left side of the model. Periodic boundary condition was applied to the top and bottom end of the model. Injected liquids were water and olive oil, and their properties described in Section 2 were used. The Morse-type inter-particle potential model, Eq. (9), was considered for interaction between the fluid and solid particles, and parameters listed in Table 1 were used. For simplicity and stability of the analysis,

the density of air was set to the same value of water, and its kinetic viscosity was 1.515×10^{-5} m^2/s. The inter-particle force was not applied to air particles. The void fraction was determined as the number of air particles divided by the initial number of particles in the designated region.

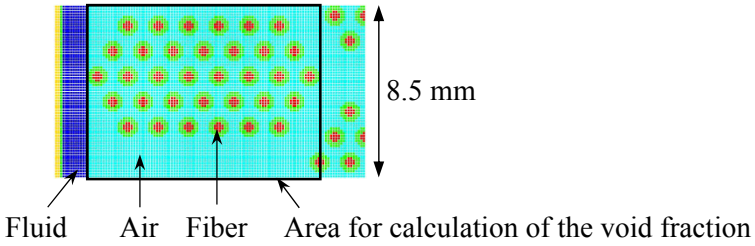

Figure 5. Analytical model of flow to a fiber bundle.

Figure 6 depicts snapshots of predicted impregnation process with water. When water reached the left end of the bundle (Fig. 6a), the shape of the flow front coincided with the experiment. The bundle was hardly immersed in the injection direction, and water flowed mainly between the bundles (Figs. 6b and 6c). The bundle was surrounded by water before the space between fibers was completely filled, and void was finally formed in the bundle (Fig. 6d). This process of micro-void formation agreed well with the experiment. The predicted void fraction at the final state (9.4%) was lower than the experiment, since impregnation proceeded slightly in the direction perpendicular to the injection.

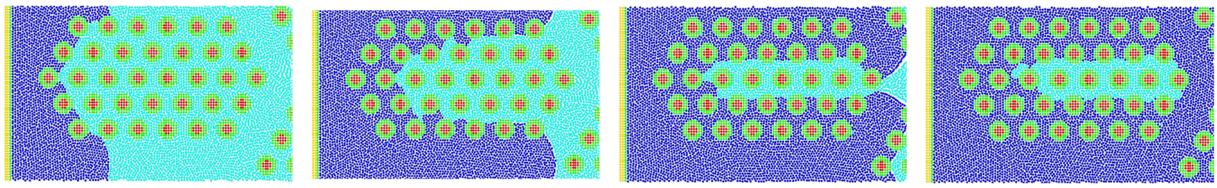

Figure 6. Analytical result of the water flow to a fiber bundle.

Figure 7 presents snapshots of predicted olive oil flow. Similar to the experiment in Section 2, impregnation proceeded from the left end of the bundle in the injection direction until 0.6 s (Figs. 7a and 7b). The bundle was also immersed in the direction perpendicular to the injection direction due to the wettability, and small amount of air was then entrapped between fibers (Fig. 7c). Flow of oil between bundles was slightly faster than infiltration of the bundle, and the bundle was surrounded by the oil before air was ejected (Fig. 7d). Although the entrapment of air differed from the experiment, most part of the bundle was filled with the oil, and the void fraction at the final state was 2.9%.

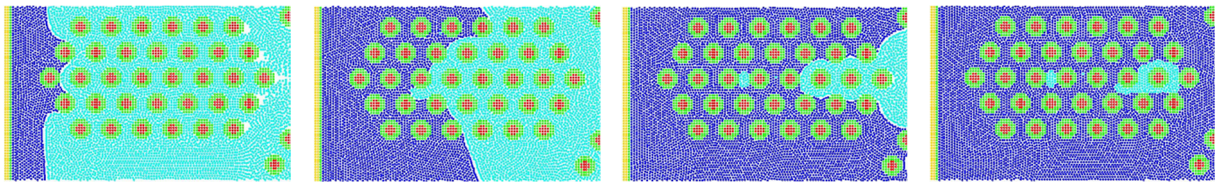

Figure 7. Analytical result of the olive-oil flow to a fiber bundle.

Although small error appeared in the predicted void fraction, overall trend of the impregnation process agreed with the experiment in Section 2. The micro-scale flow analysis to the fiber preform with an adequate wettability model will provide information about fraction of micro-voids in fiber bundles.

4.3. Influence of the molding conditions on the void content

The experiment and analysis of liquid flow to fiber bundles suggests that the process of void entrapment varies by the molding conditions. Rohatgi et al. [1] indicated experimentally that the void fraction by the RTM process was organized by the modified capillary number Ca^* defined as follows:

$$Ca^* = \frac{\mu u}{\sigma \cos\theta}, \tag{13}$$

where μ is the viscosity, u is the superficial velocity (the injection flow velocity in this study), σ is the surface tension, and θ is the contact angle.

This section predicted the void fraction in fiber bundles under various conditions. Figure 8 depicts the analytical model. The size of a particle was 2 μm, and seven particles were arranged in a hexagonal shape to represent a fiber with a diameter of 6 μm. There were 3942 particles at the initial state. Fluid particles were injected from the left end of the model, and the periodic boundary condition was applied to the top and bottom of the model. In this parametric study, the density and surface tension of the fluid were constant (1000 kg/m^3 and 7.28×10^{-2} N/m). The void fraction was predicted under 27 conditions with varying injection speed (1, 10 and 100 mm/s), viscosity (0.1, 0.5 and 1 Pa·s), and contact angle (40°, 60° and 80°). These conditions corresponded to the modified capillary number range of 1.8×10^{-2} to 7.9. The number of air particles remaining in the rectangle box designated in Fig. 8 was counted after the major flow front reached the right end of the model.

Figure 9 presents the predicted result of the relationship between the void fraction and the modified capillary number. Although slight variation appeared, the void fraction increased with increasing capillary number within the range $Ca^* > 0.02$. The void fraction became zero at a certain Ca^* less than 0.01. This trend agreed well with the reported experiment [1] of micro-void formation. Therefore, the flow analysis considering the microstructure of the preform can provide an optimal molding condition to minimize micro-voids.

However, the present analysis could not reproduce the macro-voids observed in the experiment [1]. This difference would be caused by the analytical model (Fig. 8) that disregarded the woven structure. Warp fibers will be required in the model to predict the whole relationship between the void fraction and the molding condition.

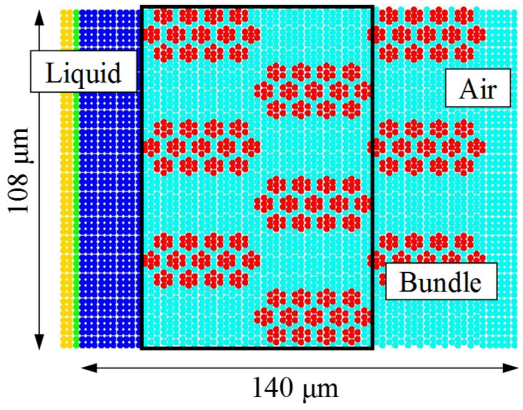

Figure 8. Analytical model to predict the void fraction under various molding conditions.

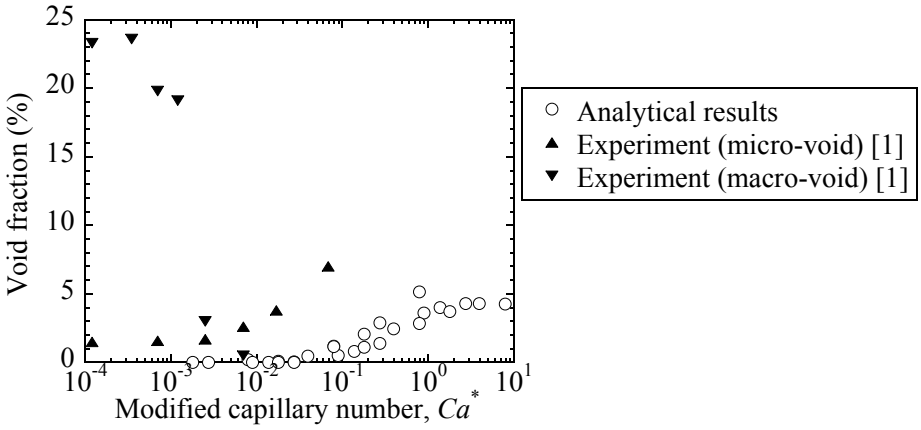

Figure 9. Relationship between the void fraction and the modified capillary number.

5. Concluding remarks

This study developed a numerical analysis predicting the liquid flow to fiber bundles and void formation in RTM by using the MPS method. The microstructure of a fiber preform was explicitly modeled by particles, and impregnation of fiber bundles with liquids was analyzed taking wettability into account. Impregnation of simulated fiber bundles was first observed via a transparent mold to clarify the void formation process by injecting water and olive oil. Although the flow velocity was the same, the void fraction when water was injected was much higher than that by the olive oil injection. This difference was caused by the wettability of liquids to the fiber material. The impregnation process was then predicted numerically, and the developed analysis with an adequate inter-particle potential force for wettability agreed well with the observation. Finally, the relationship between the void fraction and the modified capillary number was predicted, and the obtained result agreed well with the reported experiment [1] of micro-void formation. Therefore, the microscale flow analysis with considering the microstructure of the preform enables us to determine an optimal molding condition to minimize micro-void content.

Acknowledgments

S. Y. acknowledges the support of the Japan Science and Technology Agency through the Cross-ministerial Strategic Innovation Promotion Program (SIP).

References

[1] V. Rohatgi, N. Patel, and L. James. Experimental investigation of flow-induced microvoids during impregnation of unidirectional stitched fiberglass mat. *Polymer Composites*, 17:161-170, 1996.
[2] S. Koshizuka, A. Nobe, and Y. Oka. Numerical analysis of breaking waves using the moving particle semi-implicit method. *International Journal for Numerical Methods in Fluids*, 26:751-769, 1998.
[3] M. Tanaka, and T. Matsunaga. Stabilization and smoothing of pressure calculation for the moving particle semi-implicit method. *Journal of Computer Physics*, 229:4279-4290, 2010.
[4] M. Kondo, S. Koshizuka, and M. Takimoto. Surface tension model using inter-particle potential force in moving particle semi-implicit method. *Transactions of JSCES*, 21:20070021, 2007.